Journal of Solid State Chemistry 184 (2011) 3190–3194

Contents lists available at SciVerse ScienceDirect

Journal of Solid State Chemistry

journal homepage: www.elsevier.com/locate/jssc

Synthesis and photoluminescence properties of the high-brightness Eu^{3+}-doped $M_2Gd_4(MoO_4)_7$ (M=Li, Na) red phosphors

Chengchun Zhao [a,c], Xin Yin [b], Fuqiang Huang [b,*], Yin Hang [a,**]

[a] Key Laboratory of Materials for High Power Laser, Shanghai Institute of Optics and Fine Mechanics, Chinese Academy of Sciences, Shanghai 201800, China
[b] CAS Key Laboratory of Materials for Energy Conversion, Shanghai Institute of Ceramics, Chinese Academy of Sciences, Shanghai 200050, China
[c] Graduate School of Chinese Academy of Sciences, Beijing 100039, China

ARTICLE INFO

Article history:
Received 18 August 2011
Received in revised form
19 September 2011
Accepted 20 September 2011
Available online 4 October 2011

Keywords:
Optical materials
Luminescence
Light-emitting diodes

ABSTRACT

A series of red-emitting phosphors Eu^{3+}-doped $M_2Gd_4(MoO_4)_7$ (M=Li, Na) have been successfully synthesized at 850 °C by solid state reaction. The excitation spectra of the two phosphors reveal two strong excitation bands at 396 nm and 466 nm, respectively, which match well with the two popular emissions from near-UV and blue light-emitting diode chips. The intensity of the emission from $^5D_0$ to $^7F_2$ of $M_2(Gd_{1-x}Eu_x)_4(MoO_4)_7$ phosphors with the optimal compositions of x=0.85 for Li or x=0.70 for Na is about five times higher than that of Y_2O_3:Eu^{3+}. The quantum efficiencies of the entitled phosphors excited under 396 nm and 466 nm are also investigated and compared with commercial phosphors $Sr_2Si_5N_8$:Eu^{2+} and $Y_3A_5O_{12}$:Ce^{3+}. The experimental results indicate that the Eu^{3+}-doped $M_2Gd_4(MoO_4)_7$ (M=Li, Na) phosphors are promising red-emitting phosphors pumped by near-UV and blue light.

1. Introduction

Recently, a lot of attention has been drawn to research on white light-emitting diodes (LEDs) because of their merits of significant power saving, higher luminous efficiency, and longer lifetime compared with the incandescent or fluorescent lamps. At present, white LEDs fabricated by combining a blue LED chip with a yellow-emitting phosphor (YAG:Ce^{3+}) is commercially available due to the unsurpassed efficiency such a combination provides [1–3]. However, they exhibit poor color rendering index (CRI) and high correlated color temperature due to the deficiency of red emission. One solution to this problem is to excite red, green and blue phosphors by UV LED. However, current sulfide and oxysulfide for red phosphors suffer chemical instability and decompose at high temperature, whereas Eu^{2+}-doped nitrides phosphors such as $CaAlSiN_3$ suffer from a relatively difficult preparation process [4]. Red-emitting phosphors with excellent performance are urgently required.

In recent years, Eu^{3+} doped molybdates have received much attention because of their low synthesis temperature, high red-emitting efficiency, and superior chemical stability [5–7]. Recently, the molybdates $M_2Gd_4(MoO_4)_7$ (M=Li, Na) have been investigated for applications in solid-state laser materials [8–10]. $Na_2Gd_4(MoO_4)_7$ is of isomorphism of $Li_2Gd_4(MoO_4)_7$. $Li_2Gd_4(MoO_4)_7$ was first reported by Pandey as ferroelectric and paramagnetic materials [11]. A subsequent publication supposed that $Li_2Gd_4(MoO_4)_7$ has a defect scheelite (space group $I4_1/a$) structure with the formula $Li_{0.286}Gd_{0.571}\square_{0.143}MoO_4$ (□ represents vacancy) [12]. It was assigned to be isostructural to the scheelite $CaWO_4$. However, the Ca^{2+} sites in $Li_2Gd_4(MoO_4)_7$ are not fully occupied by Li^+ and Gd^{3+} ions, and 14.3% of them are unoccupied. Moreover, the site symmetry of Gd^{3+} (S_4) lacks inversion center. Therefore, the two compounds could be suitable hosts for Eu^{3+}-doped phosphors with high color purity and brightness by induced $^5D_0 \rightarrow {}^7F_2$ emission. To the best of our knowledge, the synthesis and luminescence properties of Eu^{3+}-doped $M_2Gd_4(MoO_4)_7$ (M=Li, Na) phosphors have not been reported. In this work, we systemically studied the luminescence behavior of Eu^{3+}-doped $M_2Gd_4(MoO_4)_7$ (M=Li, Na) and compared their quantum efficiencies with those of commercial phosphors $Sr_2Si_5N_8$:Eu^{2+} and $Y_3A_5G_{12}$:Ce^{3+}.

2. Experimental

2.1. Sample preparation

Powder samples $Li_2(Gd_{1-x}Eu_x)_4(MoO_4)_7$ (LGM:xEu^{3+}) and $Na_2(Gd_{1-x}Eu_x)_4(MoO_4)_7$ (NGM:xEu^{3+}) were prepared by a conventional solid state method. Briefly, the starting material was a mixture of Li_2CO_3 (A.R. 99.9%), Na_2CO_3 (A.R. 99.9%), Gd_2O_3(99.99%), Eu_2O_3(99.99%), and Mo_2O_3(A.R. 99.9%). The stoichiometric amount of raw materials was thoroughly mixed by

* Corresponding author. Fax: +86 21 52413903.
** Also corresponding author.
E-mail addresses: huangfq@mail.sic.ac.cn (F. Huang), yhang@siom.ac.cn (Y. Hang).

0022-4596/$ - see front matter © 2011 Elsevier Inc. All rights reserved.
doi:10.1016/j.jssc.2011.09.025

grinding in an agate mortar, heated up to 850 °C and kept at this temperature for 5 h in air.

2.2. Sample characterization

The phase purity of LGM:xEu^{3+} and NGM:xEu^{3+} phosphors were carefully checked by using powder X-ray diffraction (XRD) analysis on a Bruker D8 Focus diffractometer with Cu$K\alpha$ radiation (λ=1.5418 Å) operated at 40 kV and 40 mA. The XRD data was collected in a 2θ range from 10° to 80°. The morphology Energy-dispersive X-ray spectroscopy (EDS) of the samples was inspected using a scanning electron microscope (SEM, JEOL JSM-6510) equipped with an energy-dispersive X-ray analyzer (EDX Oxford INCA Model 6498). The photoluminescence (PL) and photoluminescence excitation (PLE) spectra were measured with a Horiba Jobin Yvon Fluoromax-4 Spectrofluorometer. An integrating sphere (F-3018) attached to the Spectrofluormeter was used to carry out the measurements of the Commission Internationale de L'Eclairage (CIE) chromaticity coordinates and photoluminescence quantum efficiency.

3. Results and discussion

3.1. Crystal structure and morphology of the phosphors

XRD patterns of $M_2Gd_4(MoO_4)_7$ (M=Li, Na) samples with and without dopants sintered at 850 °C for 5 h are shown in Fig. 1. In this work, the concentration of Eu^{3+} is varied from x=0 to 0.95, and the XRD patterns of all samples are similar. Here, only the XRD patterns of samples with the optimal doping concentration of LGM:0.85Eu^{3+} and NGM:0.70Eu^{3+} are displayed as representatives. All peaks of the as-prepared samples can be assigned to the scheelite phase, indicating that the scheelite structure is retained after doping. The lattice parameters determined from XRD patterns are listed in Table 1. The diffraction peaks shift to lower θ values after doping because of the larger radius of Eu^{3+} compared to that of Gd^{3+}, in accordance with the Bragg equation: $\lambda=2d\sin\theta$ (Fig. 1).

The morphologies and constituent elements of the as-prepared LGM:0.85Eu^{3+} and NGM:0.70Eu^{3+} samples were investigated by the SEM and EDS. The sizes of the aggregated particles range from 3 to 8 μm (Fig. 2(a) and (c)). Moreover, a small area of each sample was selected for EDS measurement, characterizing the composition of the phosphors, as presented in Fig. 2(b) and (d). It confirms the formation of all samples by the synthesis method herein according to the presence of Na, Eu, Gd, Mo, and O. However, the light Li element was hard to identify by EDS measurement. The atomic ratio of Eu to the sum of Eu and Gd were about 0.84 and 0.69 for LGM:0.85Eu^{3+} and NGM:0.70Eu^{3+}, which agrees with that of the starting materials.

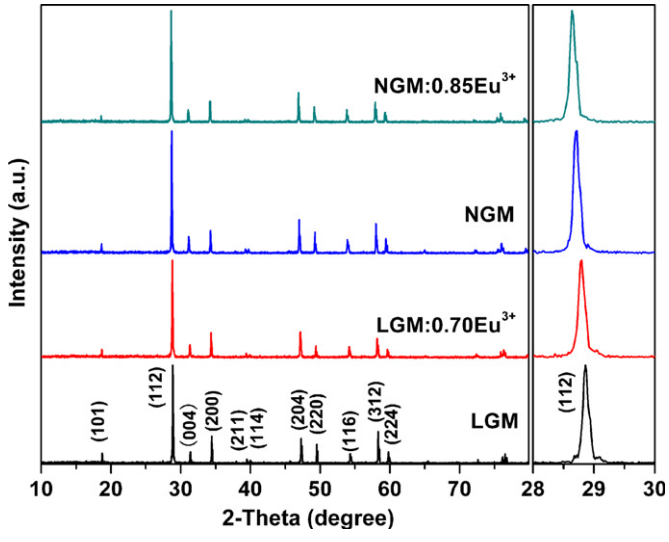

Fig. 1. Powder XRD patterns of LGM, LGM:0.85Eu^{3+}, NGM and NGM:0.70Eu^{3+} calcined at 850 °C for 5 h.

Table 1
Lattice parameters ($\alpha=\beta=\gamma=90°$) of the as-prepared LGM, LGM:0.85Eu^{3+}, NGM and NGM:0.70Eu^{3+}.

Sample	a (Å)	c (Å)	V (Å^3)
LGM	5.204	11.394	308.548
LGM:0.85Eu^{3+}	5.216	11.424	310.769
NGM	5.228	11.479	313.735
NGM:0.70Eu^{3+}	5.238	11.497	315.502

3.2. Absorption spectra and luminescence properties of LGM:Eu^{3+} and NGM:Eu^{3+} phosphors

The absorption bands from 250 nm to 370 nm in the absorption spectra of undoped LGM and NGM hosts (Fig. 3(a) and (c)) are attributed to the $(MoO_4)^{2-}$ group [13]. The broad absorption bands shift to lower energy for the doped samples (Fig. 3(b) and (d)) due to the overlap of $(MoO_4)^{2-}$ group absorption and the Eu^{3+}–O^{2-} charge transfer band (CTB). The sharp peaks in the range from 370 to 600 nm are associated with typical intra-4f forbidden transitions of the Eu^{3+} ions. The room temperature excitation spectra and emission spectra of both LGM:0.85Eu^{3+} and NGM:0.70Eu^{3+} are shown in Fig. 4.

Similar to the absorption spectra, the excitation spectra monitored at 617 nm ($^5D_0\rightarrow{}^7F_2$) can be divided into two regions: sharp lines associated with the intra-4f transitions and the charge-transfer band [14]. The shape difference between the absorption and excitation spectra in the charge-transfer band is because part of the charge-transfer absorption does not contribute to the $^5D_0\rightarrow{}^7F_2$ emission. It can be seen in Fig. 4 that LGM:0.85Eu^{3+} shows stronger blue and green-yellow excitation (from 440 nm to 550 nm) than NGM:0.70Eu^{3+}, whereas NGM:0.70Eu^{3+} shows stronger near-UV excitation (below 440 nm). The strong excitation bands located at 466 nm and 396 nm are attributed to the $^7F_0\rightarrow{}^5D_2$ and $^7F_0\rightarrow{}^5L_6$ transitions, indicating that Eu^{3+}-doped $M_2Gd_4(MoO_4)_7$ (M=Li, Na) phosphors can be used as the red phosphor excited by blue or near-UV LED chips.

On excitation with a 466 nm irradiation, the emission line ($^5D_0\rightarrow{}^7F_2$) centered at 617 nm dominated in the emission spectra. The photoluminescence (PL) intensity increases with the increase in Eu^{3+} content up to a critical concentration, after which it decreases due to concentration quenching effect. The optimal Eu^{3+} concentration in LGM and NGM are 0.85 and 0.70, and the emission intensity of the two samples is about five times higher than that of Y_2O_3:Eu^{3+} phosphor under blue excitation (Fig. 4). The photoluminescence and concentration quenching behavior will be discussed in detail later.

The emission spectra of LGM:xEu^{3+} and NGM:xEu^{3+} under 466 nm excitation are similar, as is shown in Fig. 5(a) and (b). Emission peaks at 530–545, 550–560, 579–582, 583–600, 603–635, and 645–660 nm are assigned to the $^5D_1\rightarrow{}^7F_1$, $^5D_1\rightarrow{}^7F_2$, $^5D_0\rightarrow{}^7F_0$, $^5D_0\rightarrow{}^7F_1$, $^5D_0\rightarrow{}^7F_2$, and $^5D_0\rightarrow{}^7F_3$ transitions of the Eu^{3+} ions, respectively. The emission intensity of the higher excited state ($^5D_1$) in the two hosts is very weak compared with the excited state $^5D_0$ even at low Eu^{3+} concentration. This is different from the host materials with very low phonon energy

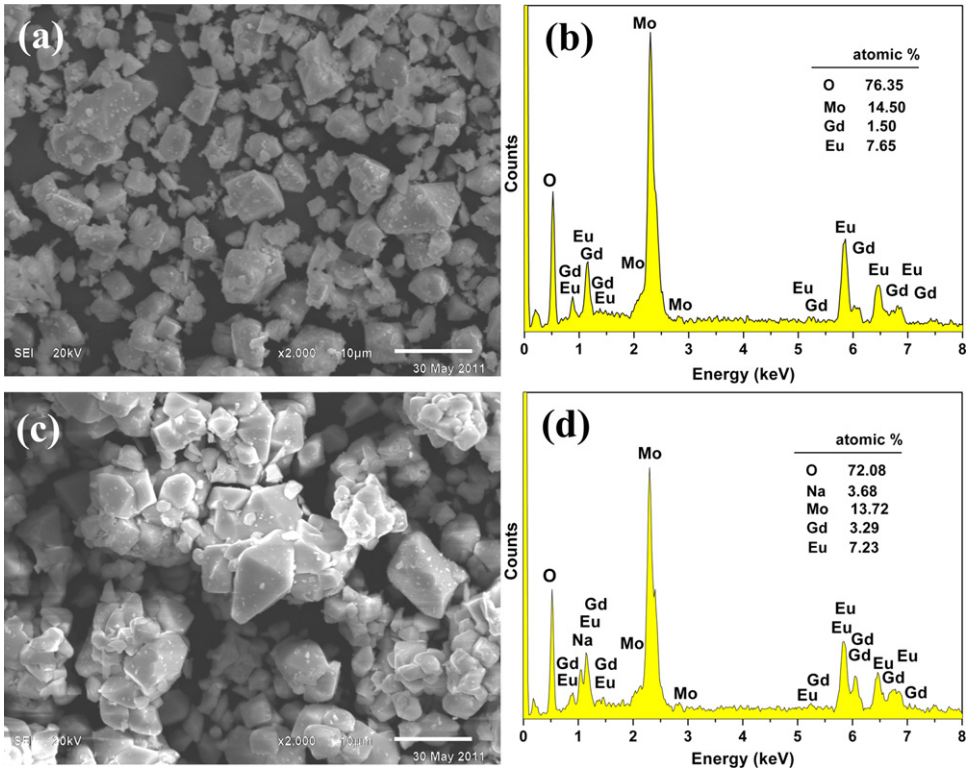

Fig. 2. SEM micrographs and EDS data of the red phosphors calcined at 850 °C for 5 h: (a, b) LGM:0.85 Eu^{3+} and (c, d) NGM:0.70 Eu^{3+}.

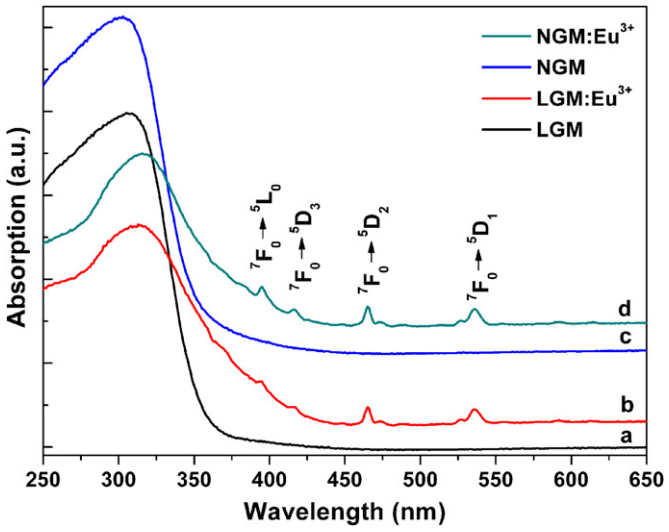

Fig. 3. Absorption spectra of the red phosphors: (a) LGM, (b) LGM:0.85Eu^{3+}, (c) NGM, and (d) NGM:0.70Eu^{3+}.

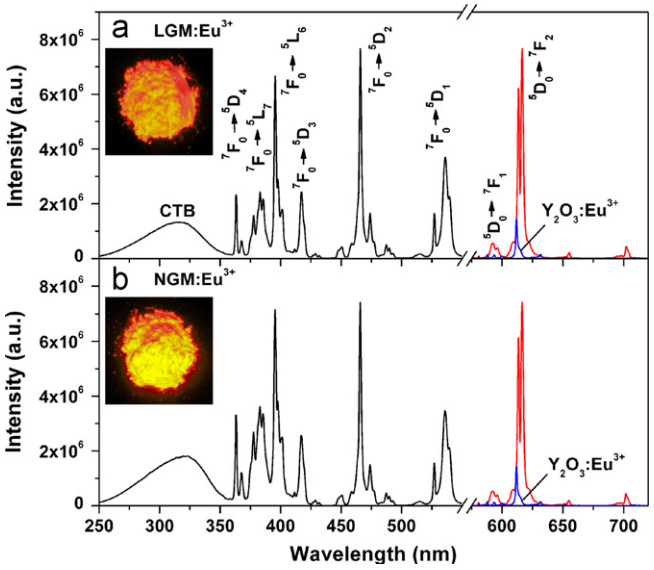

Fig. 4. Excitation (λ_{em}=617 nm) and emission (λ_{ex}=466 nm) spectra of the red phosphors: (a) LGM:0.85Eu^{3+} and (b) NGM:0.70Eu^{3+}. Emission spectra for Eu^{3+}-doped $M_2Gd_4(MoO_4)_7$ (M=Li, Na) and Y_2O_3:Eu^{3+} are represented by red and blue lines, respectively. The insets show the images of the phosphors excited at 365 nm in a UV box. The emission spectrum (λ_{ex}=468 nm) of $(Y_{0.95}Eu_{0.05})_2O_3$ is shown as comparison. (For interpretation of the references to color in this figure legend, the reader is referred to the web version of this article.)

such as $CaIn_2O_4$:Eu^{3+} [15]. One important reason is the phonon emission of $^5D_1$ state. The rate of phonon emission, W_{NR}, depends on the number of phonons emitted simultaneously to bridge the energy gap and is expressed as $W_{NR} \propto \exp(-k_B \Delta E/\hbar\omega_{max})$ [16], where ΔE is the energy gap to the nearest lower level and ω_{max} is the maximum energy of phonons coupled to the emitting states. The $CaIn_2O_4$ host has a maximum available phonon energy of about 475 cm^{-1}. On contrast, LGM and NGM hosts have a phonon energy of around 900 cm^{-1} relating to the Mo–O vibration in $(MoO_4)^{2-}$ group [17,18]. The energy gap between $^5D_1$ and $^5D_0$ is about 1700 cm^{-1}, which is only about two times of the maximum phonon energy of the hosts, so the multiphonon relaxation rate is relatively high.

Another energy path for the $^5D_1 \rightarrow {}^5D_0$ is cross-relaxation, which is also a nonradiative process. The higher emitting level $^5D_1$ transfers its energy to neighboring ions of the same species, promoting the neighboring ion from ground state to a metastable level, e.g. $^5D_1(Eu^{3+}) + {}^7F_0(Eu^{3+}) \rightarrow {}^5D_0(Eu^{3+}) + {}^7F_3(Eu^{3+})$ [16]. At higher doping concentration, Eu^{3+} ions get closer and this nonradiative process is enhanced. As a result, for LGM:$x$$Eu^{3+}$ (Fig. 5(a)), the emission intensity of $^5D_1 \rightarrow {}^7F_1$ decreases when

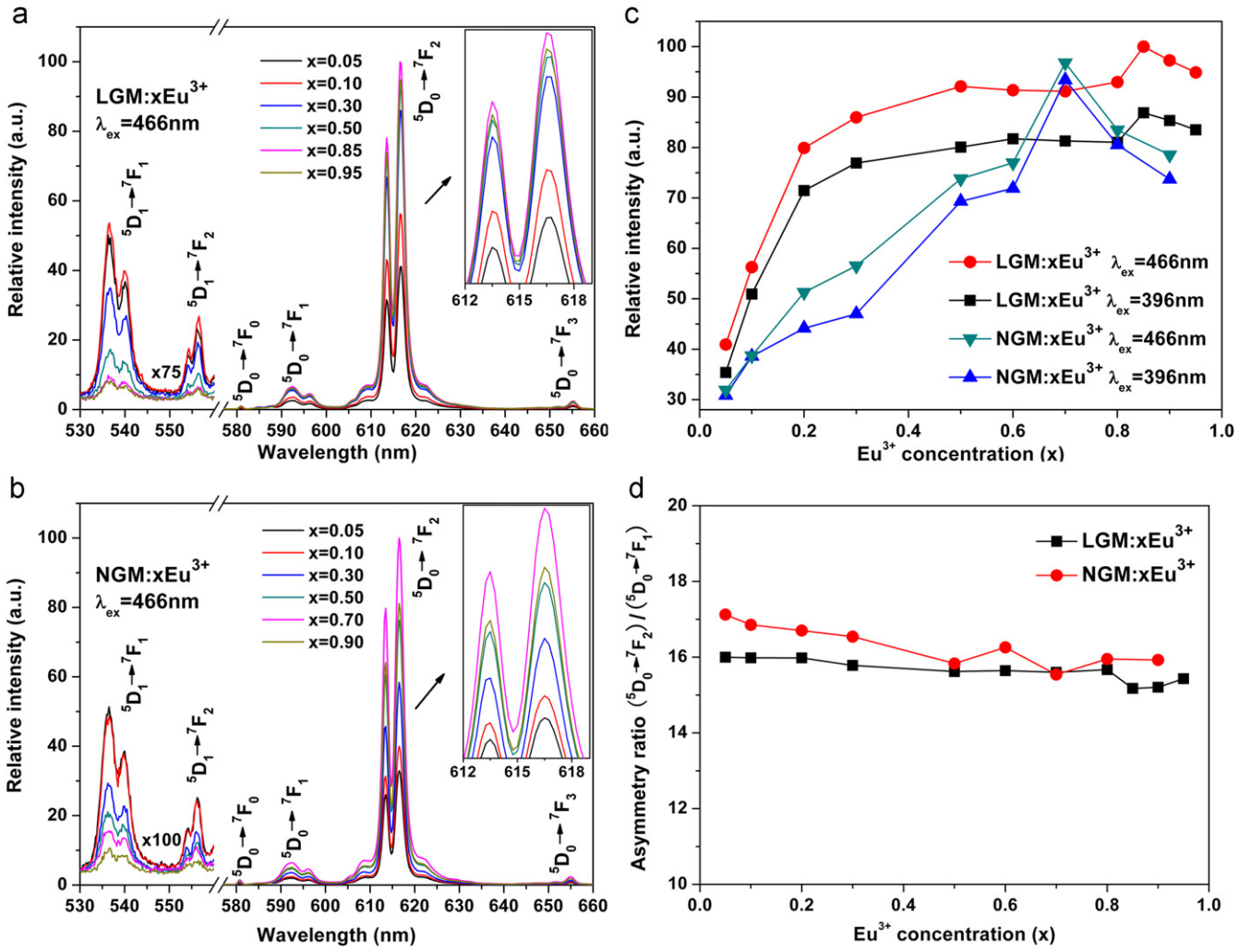

Fig. 5. Dependence of emission spectra of (a) LGM:xEu^{3+} and (b) NGM:xEu^{3+} (λ_{ex}=466 nm), and the enlarged regions in the insets. (c) Dependence of the intensity at 617 nm of LGM:xEu^{3+} and NGM:xEu^{3+}. (d) Dependence of the asymmetry ratio on Eu^{3+} ion concentration in LGM:xEu^{3+} and NGM:xEu^{3+} (λ_{ex}=466 nm).

$x>0.10$. However, this critical concentration is not higher than 0.05 for NGM:xEu^{3+} (Fig. 5(b)).

The relative emission intensity of $^5D_0\rightarrow{}^7F_2$ as a function of Eu^{3+} concentration is presented in Fig. 5(c). Before concentration quenching is reached, the intensity of emission increases with the Eu^{3+} ion concentration until x=0.85 and 0.70 for LGM and NGM, respectively. Concentration quenching is caused by the energy transfer between luminescent centers, and these energy-transfer chains trigger energy migration to the energy sink such as crystalline defects or trace ions. As the concentration of Eu^{3+} ions increases, the distance between the Eu^{3+} ions decreases, favoring the nonradiative energy transfer among Eu^{3+} ions. The high quenching concentration is caused by the scheelite-related structure, similar to other Eu^{3+}-doped molybdates. In these compounds, the bond angles of O–Mo–O and Eu–O–Mo are about 105° and 100°, respectively, leading to a long distance between Eu^{3+} ions and great difficulty for energy transfer occurrence between Eu^{3+} ions [19,20]. On the other hand, the isolated $(MoO_4)^{2-}$ groups can also block the energy transfer path. It is noticeable that the 617 nm emission intensity of LGM:xEu^{3+} increases quickly before x=0.30 but does not change significantly when $x>0.30$. On contrast, it changes gradually with increasing Eu^{3+} concentration for NGM:xEu^{3+}. Compared with LGM:0.85Eu^{3+}, NGM:0.70Eu^{3+} shows stronger red emission under 396 nm excitation, in accordance with the excitation spectra in Fig. 4. Therefore, NGM:0.70Eu^{3+} is more suitable for applications in near-UV based LEDs.

The energy levels of Eu^{3+} are weakly affected by ligand ions in the crystals because its 4f electrons are shielded by the external electric fields of the outer $5s^25p^6$ electrons. So the shape of emission line does not change with Eu^{3+} ion concentration in LGM and NGM. However, the electric dipole transition $^5D_0\rightarrow{}^7F_2$, which is utilized for practical applications, is strongly influenced by the coordination environment, whereas the magnetic dipole transition $^5D_0\rightarrow{}^7F_1$ is insensitive to that. The electric dipole emission around 603–635 nm, much stronger than the magnetic dipole transition centered at 592 nm, is induced by the lack of inversion symmetry at the Eu^{3+} site. So the $(^5D_0\rightarrow{}^7F_2)/(^5D_0\rightarrow{}^7F_1)$ emission ratio can be used as an index to measure the site symmetry of Eu^{3+} ions. The dependence of the $(^5D_0\rightarrow{}^7F_2)/(^5D_0\rightarrow{}^7F_1)$ emission ratio on Eu^{3+} ion concentrations in LGM:xEu^{3+} and NGM:xEu^{3+} under excitation at 466 nm is shown in Fig. 5(d). The asymmetry ratio of the two phosphors nearly keeps constant at 16 for different Eu^{3+} concentrations. The ratio is about two times more than those of Eu^{3+}-doped $Y_2(MoO_4)_3$ (8.3) [6] and $Li_3Ba_2Gd_3(MoO_4)_8$ (8.1) phosphors [7]. At the same time, emission intensities of $^5D_0\rightarrow{}^7F_J$ (J=0, 3, 4) transitions are much weaker than that of $^5D_0\rightarrow{}^7F_1$. So the larger asymmetry ratio also implies that more excitation energy of $^5D_0$ level has contributed to the 617 nm line emission.

Table 2
Quantum efficiencies of LGM:0.85Eu^{3+} and NGM:0.70Eu^{3+} and the references at different excitation wavelengths.

Sample	Excitation wavelength (nm)	
	396	466
LGM:0.85Eu^{3+}	16.4%	23.1%
NGM:0.70Eu^{3+}	19.0%	22.6%
Eu_2O_3	1.00%	1.40%
$Sr_2Si_5N_8$:Eu^{2+}	–	18.4%
$Y_3Al_5O_{12}$:Ce^{3+}	–	38.4%

3.3. CIE chromaticity coordinates and quantum efficiencies of LGM:0.85Eu^{3+} and NGM:0.70Eu^{3+}

Under 466 nm excitation, the CIE chromaticity coordinates of the red emission of the LGM:0.85Eu^{3+} and NGM:0.70Eu^{3+} phosphors are (0.673, 0.327) and (0.672, 0.328), which are almost equal to the NTSC system standard red chromaticity (0.670, 0.330). It indicates the high color purity of both the red phosphors. These chromaticity coordinates are also better than the commercially available Y_2O_2S:Eu^{3+} red phosphor (0.624, 0.337). Furthermore, according to their excitation spectra, the LGM:Eu^{3+} and NGM:Eu^{3+} phosphors can absorb not only the emission of UV LEDs but also that of blue LEDs. Thus, they can be used to compensate the red color deficiency of YAG:Ce^{3+} or create white light by combining with a blue chip and another green phosphor.

Quantum efficiencies of the selected samples (LGM:0.85Eu^{3+}, NGM:0.70Eu^{3+}) were calculated by the method described by De Mello et al. [21] and Palsson and Monkman [22]. Briefly, the method allows determining the sample quantum efficiency Φ_f by measuring the ratio between the number of photons emitted (N_{em}) and the number of those absorbed (N_{abs}) by the sample using the relation: $\Phi_f = N_{em}/N_{abs} = (E_c - E_a)/(L_a - L_c)$, where E_c is the integrated luminescence of the sample caused by direct excitation, E_a is the integrated luminescence from an empty integrating sphere (without the sample, only a blank), L_a is the integrated excitation profile from an empty integrating sphere, and L_c is the integrated excitation profile when the sample is directly excited by the incident beam.

The quantum efficiencies of LGM:0.85Eu^{3+} and NGM:0.70Eu^{3+} together with Eu_2O_3, commercial red phosphor $Sr_2Si_5N_8$:Eu^{2+}, and commercial yellow phosphor $Y_3A_5G_{12}$:Ce^{3+} are listed in Table 2. The data were acquired under similar conditions. Compared with LGM:0.85Eu^{3+}, the quantum efficiency of NGM:0.70Eu^{3+} is higher (19.0%) under 396 nm excitation but lower (22.6%) under 466 nm excitation, which is consistent with the results in Fig. 5(c). Hence, NGM:0.70Eu^{3+} is more suitable for near-UV applications. Under 466 nm blue light excitation, the composition-optimized LGM:0.85Eu^{3+} and NGM:0.70Eu^{3+} exhibit high quantum efficiency, about 125% of the commercial red-emitting compound $Sr_2Si_5N_8$:Eu^{2+} and 60% of the commercial yellow phosphor $Y_3A_5G_{12}$:Ce^{3+}. What is more, Eu^{3+}-doped LGM and NGM phosphors can be successfully prepared at only 850 °C. These results indicated that LGM:0.85Eu^{3+} and NGM:0.70Eu^{3+} may serve as potential candidates for UV and blue LED applications.

4. Conclusions

In summary, we have reported the synthesis and the luminescence properties of the red phosphors Eu^{3+}-doped $M_2Gd_4(MoO_4)_7$ (M=Li, Na). The optimal doping concentration of Eu^{3+} in the Li and Na hosts are 0.85 and 0.70, respectively. The asymmetry ratio of the two phosphors nearly keeps constant at 16, about two times larger than those of Eu^{3+}-doped $Y_2(MoO_4)_3$ and $Li_3Ba_2Gd_3(MoO_4)_8$. LGM:0.85Eu^{3+} and NGM:0.70Eu^{3+} have a high color purity with CIE chromaticity coordinates of (0.673, 0.327) and (0.672, 0.328), which are close to the NTSC system standard for red chromaticity. LGM:0.85Eu^{3+} and NGM:0.70Eu^{3+} achieved a high quantum efficiency of up to 23.1%. Therefore, the Eu^{3+}-doped $M_2Gd_4(MoO_4)_7$ (M=Li, Na) red phosphors may have a potential application for white light-emitting diodes.

Acknowledgments

Financial supports from National 973 Program of China Grant nos. 2009CB939903 and 2007CB936704, NSF of China Grant nos. 10775171, 61076062 and 50902143, the State Key Program for Basic Research of China (Grant no. 2010CB630703), and Science and Technology Commission of Shanghai Grant nos. 10520706700, 0952nm06500 and 10JC1415800 are acknowledged.

References

[1] S. Lee, S.Y. Seo, J. Electrochem. Soc. 149 (2002) J85–J88.
[2] D. Haranath, H. Chander, P. Sharma, S. Singh, Appl. Phys. Lett. 89 (2006) 173118.
[3] R. Kasuya, A. Kawano, T. Isobe, Appl. Phys. Lett. 91 (2007) 111916.
[4] K. Uheda, N. Hirosaki, Y. Yamamoto, A. Naito, T. Nakajima, H. Yamamoto, Electrochem. Solid State Lett. 9 (2006) H22–25.
[5] Y.S. Hu, W.D. Zhuang, H.Q. Ye, D.H. Wang, S.S. Zhang, X.W. Huang, J. Alloy Compd. 390 (2005) 226–229.
[6] Y. Tian, X.H. Qi, X.W. Wu, R.N. Hua, B.J. Chen, J. Phys. Chem. C 113 (2009) 10767–10772.
[7] Y.C. Chang, C.H. Liang, S.A. Yan, Y.S. Chang, J. Phys. Chem. C 114 (2010) 3645–3652.
[8] H.M. Zhu, Y.F. Lin, Y.J. Chen, X.H. Gong, Q.G. Tan, Z.D. Luo, Y.D. Huang, J. Appl. Phys. 102 (2007) 063104.
[9] H.M. Zhu, Y.J. Chen, Y.F. Lin, X.H. Gong, J.S. Liao, X.Y. Chen, Z.D. Luo, Y.D. Huang, J. Phys. D-Appl. Phys. 40 (2007) 6936–6941.
[10] W. Zhao, Z.B. Lin, L.Z. Zhang, G.F. Wang, J. Alloy Compd. 509 (2011) 2815–2818.
[11] R.K. Pandey, J. Phys. Soc. Jpn. 36 (1974) 177–178.
[12] L.H. Brixner, J. Phys. Soc. Jpn. 38 (1975) 1218.
[13] M.M. Haque, H.I. Lee, D.K. Kim, J. Alloys Compd. 481 (2009) 792–796.
[14] G. Blasse, B.C. Grabmaier, Luminescent Materials, Springer-Verlag, Berlin, Germany, 1994.
[15] X.M. Liu, C.K. Lin, J. Lin, Appl. Phys. Lett. 90 (2007) 081904.
[16] W.M. Yen, S. Shionoya, H. Yamamoto, Phosphor Handbook, 2nd ed., Boca Raton, FL, 2006.
[17] W. Paraguassu, A.G. Souza, M. Maczka, P.T.C. Freire, F.E.A. Melo, J. Mendes, J. Hanuza, J. Phys.-Condens. Matter 16 (2004) 5151–5161.
[18] B.A. Kolesov, L.P. Kozeeva, J. Struct. Chem. 34 (1993) 534–539.
[19] D.L. Dexter, J.H. Schulman, J. Chem. Phys. 22 (1954) 1063–1070.
[20] C.H. Chiu, C.H. Liu, S.B. Huang, T.M. Chen, J. Electrochem. Soc. 155 (2008) J71–J78.
[21] J.C. De Mello, H.F. Wittmann, R.H. Friend, Adv. Mater. 9 (1997) 230–232.
[22] L.O. Palsson, A.P. Monkman, Adv. Mater. 14 (2002) 757–758.